Resource

Cell Reports

Pancreatic Islet Blood Flow Dynamics in Primates

Graphical Abstract

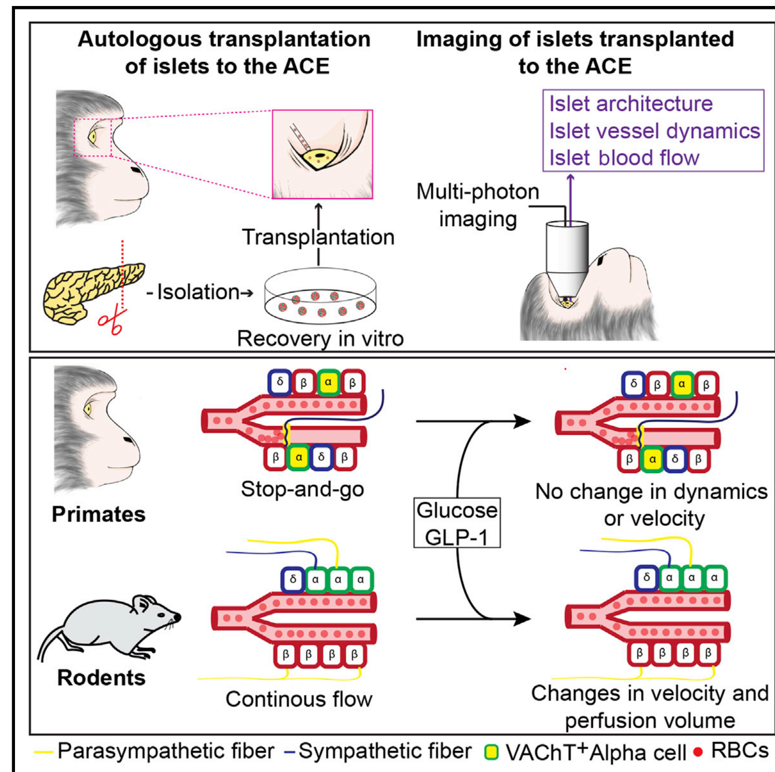

Highlights

- Monkey islets transplanted autologously into the anterior chamber of the eye (ACE)
- Monkey ACE islets imaged in vivo, longitudinally, and at single-cell resolution
- Monkey islet blood flow is dynamic and unaffected by glucose/liraglutide treatment
- Directional blood flow may be explained by islet structure-function relationship

Authors

Juan A. Diez, Rafael Arrojo e Drigo, Xiaofeng Zheng, ..., George J. Augustine, Veluchamy A. Barathi, Per-Olof Berggren

Correspondence

per-olof.berggren@ki.se

In Brief

Diez et al. establish an in vivo imaging platform where monkey islets transplanted autologously into the anterior chamber of the eye are monitored non-invasively, longitudinally, and at single-cell resolution. In contrast with mice, blood flow in primate islets is highly dynamic and unaffected by glucose or the GLP-1 analog liraglutide.

Diez et al., 2017, Cell Reports *20*, 1490–1501
August 8, 2017 © 2017 The Author(s).
http://dx.doi.org/10.1016/j.celrep.2017.07.039

CellPress

OPEN ACCESS
CellPress

Cell Reports
Resource

Pancreatic Islet Blood Flow Dynamics in Primates

Juan A. Diez,[1,2,12] Rafael Arrojo e Drigo,[1,2,3,12] Xiaofeng Zheng,[1,2] Olga V. Stelmashenko,[1,2] Minni Chua,[1] Rayner Rodriguez-Diaz,[4] Masahiro Fukuda,[1,5] Martin Köhler,[6] Ingo Leibiger,[6] Sai Bo Bo Tun,[2] Yusuf Ali,[1] George J. Augustine,[1,7] Veluchamy A. Barathi,[2,8,9] and Per-Olof Berggren[1,2,6,10,11,13,*]

[1]Lee Kong Chian School of Medicine, Nanyang Technological University, Singapore 637553, Singapore
[2]Translational Pre-Clinical Model Platform, Singapore Eye Research Institute (SERI), Singapore General Hospital, Singapore 168751, Singapore
[3]Nanyang Institute of Structural Biology (NISB), Nanyang Technological University, Singapore 636921, Singapore
[4]Division of Endocrinology, Diabetes and Metabolism, Department of Medicine, University of Miami Miller School of Medicine, Miami, FL 33136, USA
[5]Department of Molecular Therapy, National Institute of Neuroscience, National Center of Neurology and Psychiatry, Kodaira, Tokyo 187-8551, Japan
[6]The Rolf Luft Research Center for Diabetes and Endocrinology, Karolinska Institutet, Karolinska University Hospital L1, 171 76 Stockholm, Sweden
[7]Institute of Molecular and Cell Biology, A*STAR, Singapore 138673, Singapore
[8]Ophthalmology and Visual Sciences Academic Clinical Program, DUKE-NUS Graduate Medical School, Singapore 169856, Singapore
[9]Department of Ophthalmology, Yong Loo Lin School of Medicine, National University of Singapore, Singapore
[10]Imperial College London, London SW7 2AZ, UK
[11]Diabetes Research Institute, University of Miami Miller School of Medicine, Miami, FL 33136, USA
[12]These authors contributed equally
[13]Lead Contact
*Correspondence: per-olof.berggren@ki.se
http://dx.doi.org/10.1016/j.celrep.2017.07.039

SUMMARY

Blood flow regulation in pancreatic islets is critical for function but poorly understood. Here, we establish an in vivo imaging platform in a non-human primate where islets transplanted autologously into the anterior chamber of the eye are monitored non-invasively and longitudinally at single-cell resolution. Engrafted islets were vascularized and innervated and maintained the cytoarchitecture of in situ islets in the pancreas. Blood flow velocity in the engrafted islets was not affected by increasing blood glucose levels and/or the GLP-1R agonist liraglutide. However, islet blood flow was dynamic in nature and fluctuated in various capillaries. This was associated with vasoconstriction events resembling a sphincter-like action, most likely regulated by adrenergic signaling. These observations suggest a mechanism in primate islets that diverts blood flow to cell regions with higher metabolic demand. The described imaging technology applied in non-human primate islets may contribute to a better understanding of human islet pathophysiology.

INTRODUCTION

Islets of Langerhans are specialized mini-organs whose main function is to accurately control blood glucose concentration (Unger and Orci, 2010). In this important homeostatic control, insulin-secreting β cells take center stage. In addition to glucose, these cells are regulated by complex autocrine and paracrine signaling mechanisms (Cabrera et al., 2006; Jacques-Silva et al., 2010; Rodriguez-Diaz et al., 2011a; Visa et al., 2015; Watts et al., 2016; Yan-Do et al., 2016). Also, vascularization and innervation play important roles in determining the pattern of islet activity (Arrojo e Drigo et al., 2015; Lammert, 2001; Rodriguez-Diaz et al., 2011b). In fact, the interaction between sympathetic nerve fibers and contractile elements in blood vessels of human islets may imply a regulatory mechanism that coordinates blood flow with metabolic activity in the islet (Rodriguez-Diaz et al., 2011b). To date, however, this mechanism has not been experimentally proven, in part because of the inaccessibility of the islets embedded in the pancreas. Another factor is that most islet research has been done in rodents, an animal model that falls short of reproducing human physiology in health and disease. Thus, in humans, these hurdles have hampered the ability to monitor islet plasticity during the course of diabetes and to evaluate the long-term effect of anti-diabetes drugs on islets. This is, for instance, underscored by recent findings using a humanized mouse model showing compromised function of human islets and, thereby, impaired glucose homeostasis after long-term exposure to the glucagon-like peptide 1 (GLP-1) receptor agonist liraglutide (Abdulreda et al., 2016). GLP-1 has also been reported to reduce the effect of glycemia on rodent islet blood flow (Svensson et al., 2007; Wu et al., 2012). It is therefore essential to develop a longitudinal in vivo imaging platform able to monitor human islet function and survival in a setting where all other structural components (namely, the islet vasculature and innervation) are also present and functional.

As a close surrogate model of humans, the non-human primate represents an optimal platform to investigate islet biology with a direct translational effect on the human clinical setting. Monkey islets have a human-like structure and physiology; i.e., a cytoarchitecture with an intermingled endocrine cell organization,

This is an open access article under the CC BY-NC-ND license (http://creativecommons.org/licenses/by-nc-nd/4.0/).

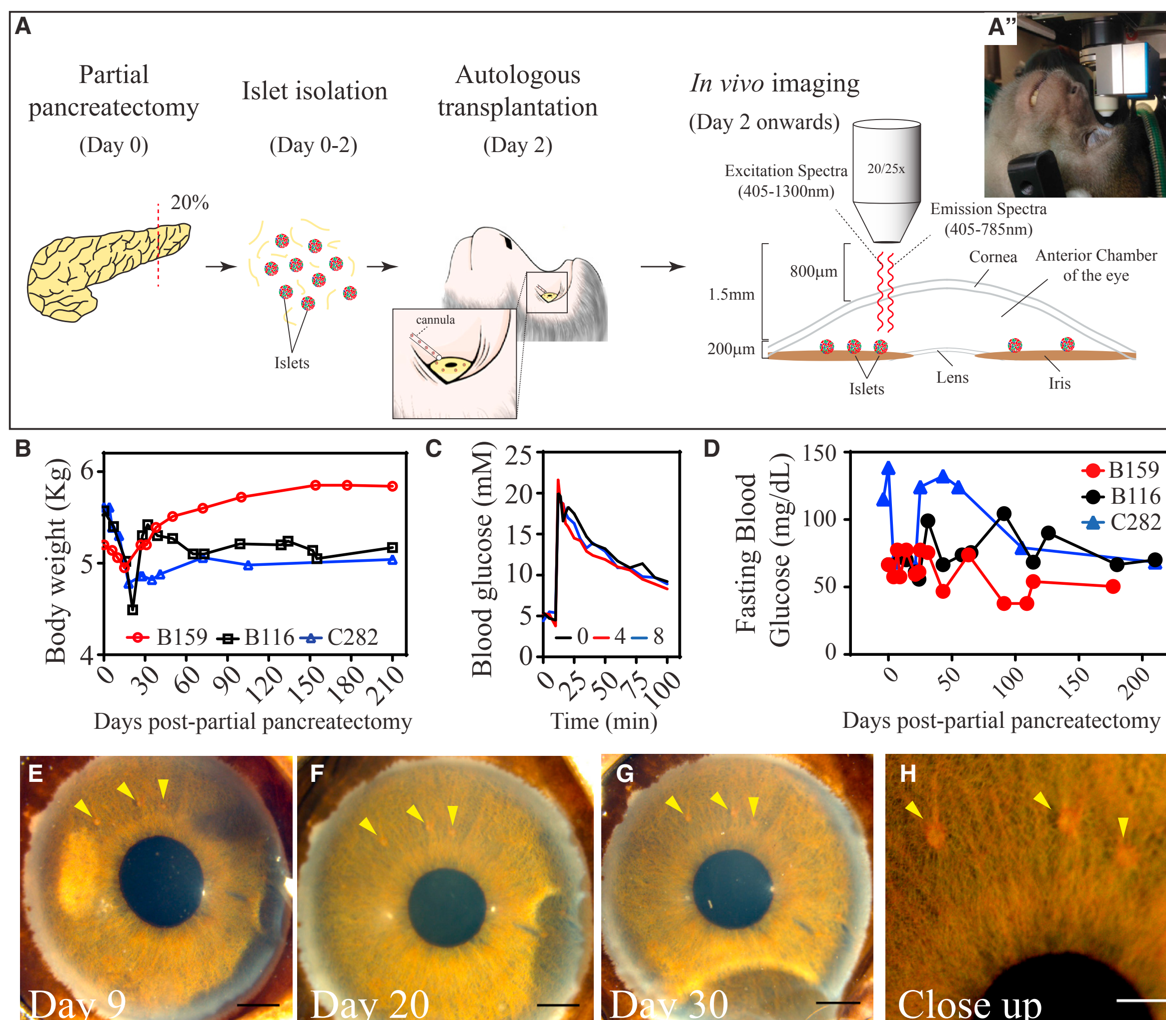

Figure 1. Autologous Islet Transplantation into the ACE

(A) Illustration of the experimental workflow used for the autologous transplantation and two-photon imaging of islets in the monkey ACE. The inset (A'') shows an anesthetized monkey placed under the objective turret.

(B) Body weight of three monkeys, B159 (red circles), B116 (black squares), and C282 (blue triangles), after partial pancreatectomy and autologous islet transplantation (performed on day 0).

(C) Intravenous glucose tolerance test (IVGTT) of a monkey before (0) (black) and 4 (red) and 8 (blue) weeks after partial pancreatectomy.

(D) Fasting blood glycemia of three monkeys (B159 in red, B116 in black, and C282 in blue) after partial pancreatectomy.

(E–H) The same three islets (arrowheads) on days 9 (E and H), 20 (F), and 30 (G) post-transplantation, seen under a stereomicroscope. Scale bars, 4 mm (E–G) and 1 mm (H).

sympathetic innervation of blood vessels, similar paracrine networks, and the same glucose response patterns (Figures 4D–4E; Figure S1 and S3A–S3D; Brissova et al., 2005; Cabrera et al., 2006; Rodriguez-Diaz et al., 2011a, 2011b). Notably, monkeys mirror several aspects of human pathophysiology, including the development of type 2 diabetes as a consequence of aging or high-fat diet feeding (Pound et al., 2014).

Here we have developed an in vivo imaging platform that combines autologous transplantation of non-human primate islets into the anterior chamber of the eye (ACE) with high-resolution two-photon microscopy, using the cornea as a natural body window, thus granting insight into the dynamics of islet blood flow in a human-like system. Given the important clinical relevance of islet blood flow and, in particular, hemodynamic stress as a putative target for therapeutic intervention in diabetes, we focused on the extent to which glucose and liraglutide affect islet blood flow in primates.

RESULTS

Autologous Islet Transplantation into the ACE

We isolated monkey islets after partial pancreatectomy of approximately 20% of the organ mass (modified from Berman et al., 2009; Figure 1A shows a schematic of the process). Islet

function was tested in vitro by measuring insulin secretion and Ca^{2+} oscillations after glucose challenge (Figure S1). Islets were kept in culture for 48 hr and then transplanted into the ACE of the same pancreatectomized animal, preventing immunological graft rejection (n = 3 separate animals). The surgical procedures did not affect body weight, glucose response, glycemic control, or health of the recipient eye in a period of over 200 days post-transplantation (Figures 1B–1D; Table S1). The transient drop in weight of the animals following partial pancreatectomy was due to post-operation discomfort and the subsequent lack of appetite. However, the animals eventually recovered their pre-operation body weight. The transplanted islets were clearly visible using a stereomicroscope, even though they were covered by a layer of pigmented iris cells approximately 4 days post-transplantation (Figures 1E–1H).

Longitudinal In Vivo Imaging of Pancreatic Islets

To perform in vivo imaging in anesthetized monkeys, we designed an upright two-photon microscope that supports the large dimensions of monkeys (Figures 2A–2D). We minimized involuntary head and eye movements using a custom-made helmet and an ‘‘eye-stabilizing ring’’ attached to the scanning stage (Figure 2C). In vivo imaging sessions started 3 days post-transplantation using a stereomicroscope (Figures 1E–1H) and the two-photon microscope (Figure 2E). Occasional 1- to 5-μm drifts in all XYZ directions because of light-triggered iris reflexes and the heartbeat of the animal were corrected with a post hoc alignment plug-in (Figure S2). To follow islet engraftment in the ACE, we imaged islet re-vascularization by using fluorescein-tagged, 150-kDa fluorescein isothiocyanate (FITC)-dextran, routinely used for labeling blood flow (Almaça et al., 2014), injected through a catheter placed in the femoral artery. In all animals studied, islet re-vascularization started between 4 and 10 days after islet transplantation, and, as occurs in mice (Speier et al., 2008), islet re-vascularization was initiated by large-diameter vessels, followed by progressive vessel branching and reduced overall vessel size (Figures 2E–2G). These results are in agreement with our previous studies, confirming that vascularization of islets engrafted in the ACE is similar to that of islets in situ in the pancreas (Ilegems et al., 2013; Perez et al., 2011; Speier et al., 2008).

Blood Flow Measurement

When the islets were fully vascularized, approximately 30 days post-transplantation, we investigated the islet blood flow pattern. Time-lapse images taken from different vascular branches in engrafted islets revealed intermittent changes in islet blood flow velocity. These changes included the stop of blood flow in some branches of the islet vasculature that lasted tens of seconds (Figure 3; Movies S1, S2, and S3). Figures 3B–3I show images of the blood flow pattern in two interconnected capillaries (corresponding to the yellow square in Figure 3A). In this representative sample, two capillaries (vessels 1 and 2; Figures 3B–3I) shared a common capillary ‘‘root’’ (Figure 3A) and initially displayed a similar blood flow velocity (Figure 3J). We observed a sudden stop in blood flow in vessel 1 that coincided with a 2-fold increase in blood flow velocity in vessel 2 (Figure 3J), which likely reflects re-routing of blood flow to vessel 2. Approximately 30 s later, blood flow resumed in vessel 1, and both vessels synchronized their blood flow velocity (Figure 3J). This phenomenon was not limited to small capillaries, occurring also in large branches of the islet vasculature (Movie S2). In contrast, similar blood flow dynamics did not occur in mouse islets transplanted into the ACE of recipient mice (Figures 3K and 3L; Movie S3). In this experimental setting, the engrafted islets are re-vascularized in part with iris-borne vessels (Nyqvist et al., 2011), and, therefore, we tested whether the dynamic blood flow observed in the engrafted monkey islets was due to an intrinsic property of the monkey iris vasculature. After monitoring the blood flow pattern in single and branched capillaries of the monkey iris, close to the engrafted islets, we did not observe any significant change in blood flow velocity (Movie S4).

Furthermore, in two independent observations, we detected events of localized vasoconstriction of islet capillaries, where the diameter of a specific section in the capillary was reduced by approximately 40% in approximately 5 s. This vaso-constricting event occurred without changes in diameter in other areas of the same or a different capillary and was not due to changes in focal plane (Figures 3M–3Q, capillary c). These results are likely explained by the existence of sphincter-like constricting mechanisms located in various capillaries around the islet (Rodriguez-Diaz et al., 2011b) that would respond to changes in the metabolism of the surrounding cells (Figure 3R). This is supported by earlier findings describing that an acute rise in circulating glucose levels leads to an increase in blood flow velocity specifically in the islet in situ (Nyman et al., 2008, 2010; Svensson et al., 2007; Wu et al., 2012). Furthermore, it has been hypothesized that such an increase in islet blood supply is a response to a higher metabolic demand from islet cells; namely, β cells (Jansson and Hellerström, 1983). Previous studies indicated that important aspects of the mouse islet vascular structure-function are retained when islets are transplanted to the ACE (Almaça et al., 2014; Speier et al., 2008). Therefore, we tested whether a similar glucose-sensitive mechanism described in rodent islets exists in primate ACE islets.

First, we determined the basal blood flow velocity in different islet and iris capillaries in fasted monkeys and observed that islet flow velocity is not dependent on fasting blood glucose levels (Figure 4A). Next, and following acquisition of basal islet and iris capillary blood flow velocities, we injected either saline or liraglutide intravenously (1 mg/kg of body weight, within the range recommended for humans and higher than the dose used in a humanized mouse model [0.3 mg/kg/day]; Abdulreda et al., 2016), followed by glucose (0.5 g/kg of body weight) 10 min later, and measured the blood blow velocities in the exact same capillaries as those used for the baseline measurements. The results obtained from two animals imaged in seven separate imaging sessions (n = 4 sessions with liraglutide and n = 3 sessions with saline) revealed a lack of a significant effect of glucose and/or liraglutide on islet blood flow velocity in monkey islets (Figure 4B). To test whether the absence of a blood flow response to glucose and/or liraglutide was due to lack of sensitivity in our imaging platform, we injected a low dose of the vasoactive catecholamine hormone epinephrine (0.15 mg, intravenously [i.v.]). In the body, epinephrine is important in

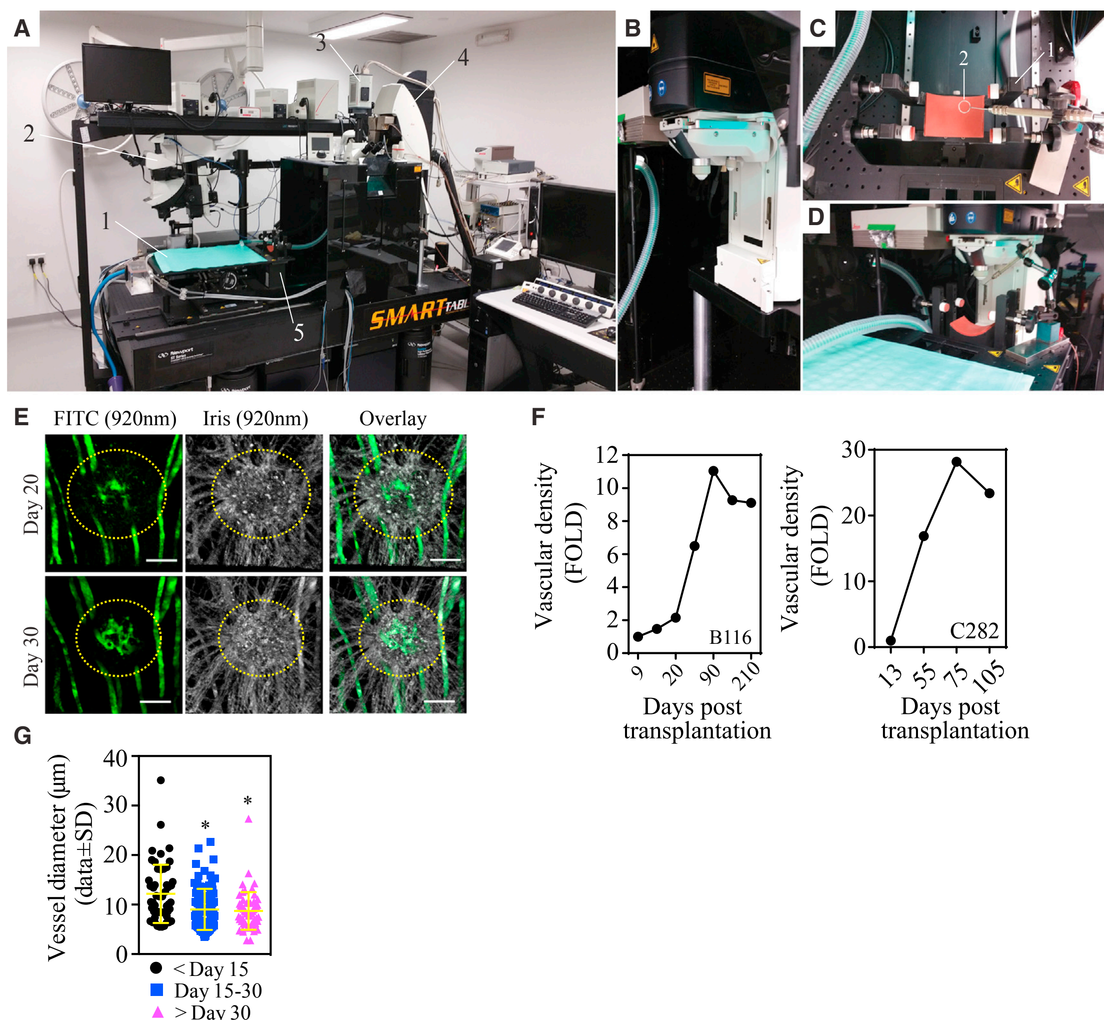

Figure 2. High-Resolution In Vivo Longitudinal Imaging of Islet Re-vascularization in the ACE of Monkeys

(A) Overview of the in vivo imaging rig setup based on the Leica SP8 microscope that can accommodate monkeys under the objective holder (for a full description and dimensions, see Experimental Procedures). 1, manual mechanical jack setup on top of a high-precision scanning stage with a heating mat to maintain the animal's core temperature at 37°C. 2, M250 Leica stereomicroscope setup on a boom stand that swings on/off the top of the scanning stage. 3, high-speed Hamamatsu electron multiplier charge-coupled device (EMCCD) camera used for wide-field microscopy. 4, confocal and two-photon scanning head. 5, custom-built head holder attached to the scanning stage and used to accommodate and stabilize the monkey's head comfortably. Below the scanning head, the light protection box can be seen, with the integrated setup (green tubing) for ventilated anesthesia used during imaging sessions.

(B) Close-up view of the inside of the light protection box, showing the microscope body with the transmitted light removed and ample space under the objective holder. The anesthesia tubes can be seen entering the box in the back.

(C) Close-up top view of the scanning stage fitted with the head (1) and eye (2) holders.

(D) Close-up view of the complete setup under the objective holder. In the top left corner, the enclosure for 2 external non-descanned detectors can be seen.

(E) Longitudinal confocal imaging of the re-vascularization process of islets engrafted in the eye of monkeys on days 20 and 30 post-transplantation. Vessels (green) were stained in vivo with FITC-labeled 150-kDa dextran. The iris is shown in gray. Both vessels and the iris were imaged by fluorescence emitted after excitation by a 920-nm laser beam. The yellow dotted-line circle demarks the limits of the engrafted islet.

(F) Quantification of the islet re-vascularization process and vascular density over time from two separate animals (B116 and C282).

(G) Measurements of the vascular diameter of engrafted islets over time.

Data are shown as SEM, acquired from n = 3 animals with n = 3 islets per animal, and all data points are shown. Scale bar, 100 μm (E).

the "flight or fight" response and, in low doses, binds to mainly β-adrenergic receptors and stimulates vasodilation, thus increasing blood flow (Ehringer and Konzett, 1962). In our setup, using fasted animals, application of epinephrine led to a consistent increase in islet capillary blood flow compared with basal conditions, thus indicating that physiological changes in blood flow velocity can be detected in vivo (Figure 4B).

OPEN
ACCESS
CellPress

Characterization of Non-human Primate (NHP) Islet Cytoarchitecture

Mouse and human islets greatly differ in their cytoarchitecture, a factor that is believed to have important functional consequences (Brissova et al., 2005; Cabrera et al., 2006). Innervation from the autonomic nervous system regulates islet function, and its pattern differs between mouse and human islets. Accordingly, the cytoarchitecture of the monkey islet has been shown to mirror that of the human islet (Brissova et al., 2005; Cabrera et al., 2006). However, its innervation pattern has not been fully characterized. We thus performed a detailed immunohistological analysis of macaque pancreas to determine the innervation pattern in the islet. Cryo-preserved pancreatic sections were immunostained using antibodies against insulin, glucagon, somatostatin, the sympathetic nerve marker tyrosine hydroxylase (TH), and the parasympathetic marker vesicular acetylcholine transporter (VAChT). The islet vascularization containing actin-rich cells was visualized by phalloidin immunostaining. Monkey islets showed an intermingled location of the endocrine cells and a proportion of α, β, and δ cells similar to that of human islets (Cabrera et al., 2006; Figures S3A–S3E). Also, as in human islets, α cells expressed the cholinergic marker VAChT (Figures S3F–S3H; Rodriguez-Diaz et al., 2011a). Likewise, the sympathetic nerve fibers were sparse and targeted mainly the islet vasculature (Figures 4D–4F). Together, these observations support the idea that monkey islets have an innervation pattern similar to human islets.

Islets Engrafted into the ACE Maintain the Expression of Major Islet Hormones and a Vascular and Innervation Pattern Similar to In Situ Islets

To investigate whether the cytoarchitecture of the engrafted islets was similar to endogenous in situ pancreatic islets, we performed an immunohistological analysis of islets engrafted into the monkey iris. After a post-transplantation period of up to 210 days, the engrafted islets were covered by a thin layer of pigmented iris cells, which were clearly visible by confocal imaging using backscattered light (Figure S3I, yellow arrows). Furthermore, immunostaining of the islet grafts using anti-insulin, anti-glucagon, and anti-somatostatin antibodies confirmed that islets engrafted in the eye contained α, β, and δ cells distributed in an intermingled way, similar to the endogenous pancreas (Figures S3J–S3M). In addition, islet grafts had a similar vascular and TH-positive fiber innervation pattern as endogenous in situ islets (Figures 4J-4L, yellow arrows, and 4M and 4N). Of note, the higher background of sympathetic fibers in the islet graft is likely observed because of the high density of sympathetic nerves in the iris.

DISCUSSION

We now report a technological development where we translate the in vivo ACE imaging technology (Speier et al., 2008) to the clinically relevant human surrogate NHP for functional studies of pancreatic islet blood flow regulation. In terms of vascularization and innervation, the data demonstrate that the islet ACE microenvironment is similar to that of in situ pancreatic islets (Figure 4; Figure S3). This notion is supported by previous papers published by us and others (Almaça et al., 2014; Donáth and Adeghate, 1988; Perez et al., 2011; Rodriguez-Diaz et al., 2012; Tucker and Torres, 1992). This likely explains why islets transplanted into the ACE function similarly as bona fide pancreatic islets (Bader et al., 2016; Ilegems et al., 2013; Speier et al., 2008). The in vivo imaging in NHP described here is an important complement to previous imaging studies mainly focused on rodents, where blood flow measurements were made indirectly or using highly invasive techniques that do not allow direct and longitudinal islet imaging (Nyman et al., 2008, 2010; Svensson et al., 2007; Wu et al., 2012). Here we report repeated imaging sessions of the same capillary in NHP islets on different days and under different conditions, minimizing the measurements variability between different animals and capillaries within one islet. Notably, this in vivo platform provides access to a critical metabolic organ, the endocrine pancreas, which is otherwise unreachable for imaging in primates.

The role of contractile elements in regulating blood flow inside capillaries has been described in various organs (Petzold and Murthy, 2011; Provenza and Scherlis, 1959). In the CNS, pericytes and astrocytes are thought to regulate cerebral blood flow in response to an increase in neuronal metabolic activity, a phenomenon called functional hyperemia (Hall et al., 2014; Petzold and Murthy, 2011). Functional hyperemia may also occur in human islets because of a sphincter-like vasoconstriction of the islet's vascular bed, mediated by sympathetic input to the islet blood vessels (Rodriguez-Diaz et al., 2011b). In the present study, we provide evidence that blood flow in non-human primate islets, the closest model to humans, is dynamic and presents rapid changes in direction. This gating system is facilitated by constriction of the capillaries, most likely under the control of autonomic innervation, suggesting an intricate functional cross-talk between the islet and the nervous system.

A previous report indicates that, in in situ mouse islets, the islet blood flow can be modulated by an ''on/off'' switch in local capillaries, triggered by an acute change from a hypoglycemic to a hyperglycemic state (Nyman et al., 2010). However, contrary to this notion, the data captured using the ACE platform suggests that the capillary blood flow in NHP ACE islets is not sensitive to small or significant changes in circulating glucose levels (Figures 4A and 4B). In this in vivo setting, physiological glucose levels are associated with fast (in matter of seconds) and marked changes in blood flow velocity and capillary perfusion and diameter that were not observed in mice examined under similar in vivo imaging conditions (Figures 3 and 4). Furthermore, indirect measurements of islet blood flow in rodents treated with the GLP-1R agonist have shown that GLP-1 can modulate islet blood flow (Svensson et al., 2007; Wu et al., 2012). However, the same was not observed in NHP islets engrafted into the ACE (Figure 4B). Of note, ACE islet function can be effectively modulated by liraglutide (Abdulreda et al., 2016). Consequently, the putative therapeutic target inferred from the protective effect of GLP-1 from hemodynamic stress in rodent islets (Wu et al., 2012) may not be relevant in primate and human islets.

Our results suggest a scenario where acute changes in the metabolic demand and activity of certain areas of the primate islet (Almaça et al., 2014; Brown and Rother, 2008) may be

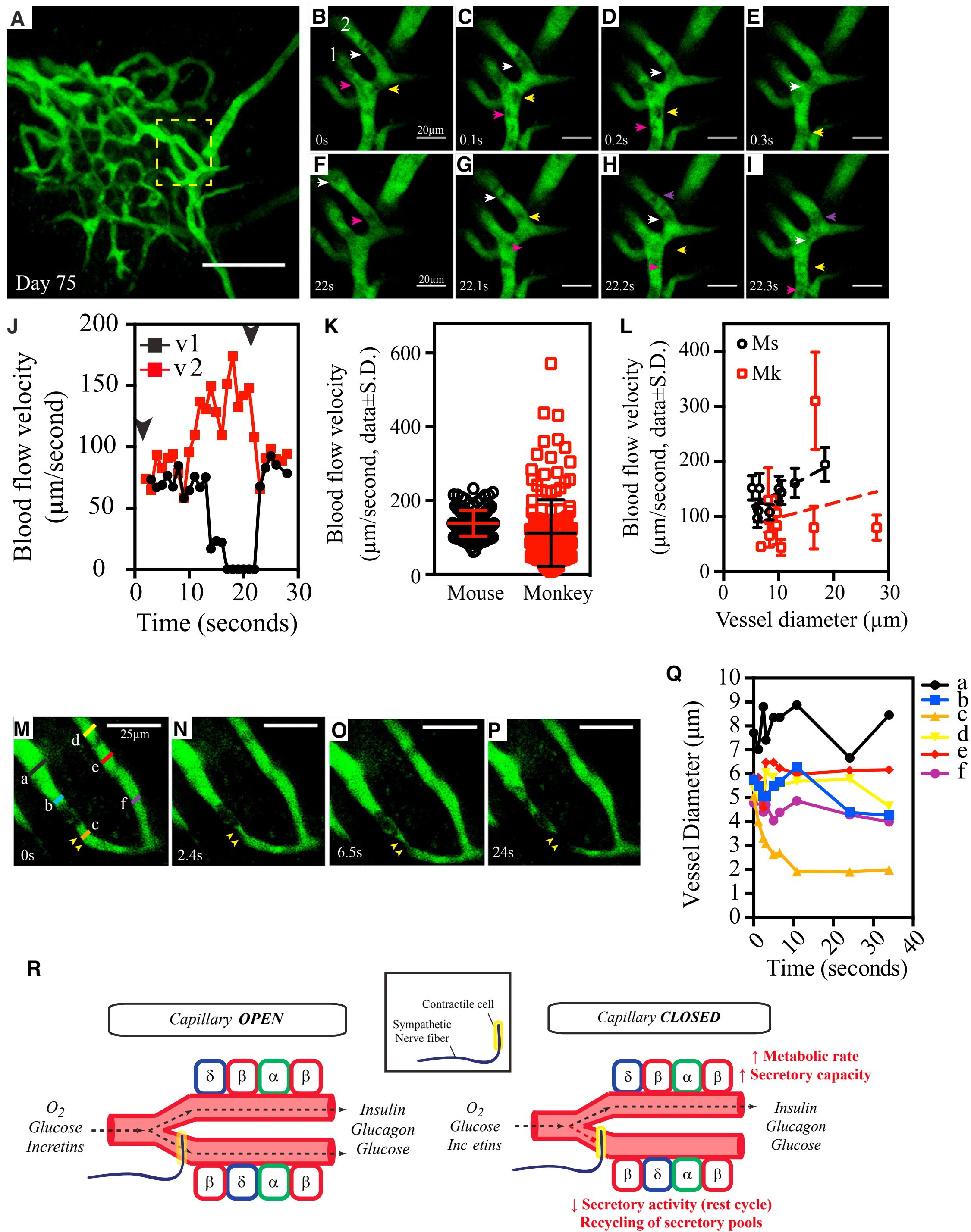

Figure 3. The Intra-islet Blood Flow Is Highly Dynamic

(A–I) Snapshots of time-lapse confocal imaging of the blood flow dynamics of two vessels (1 and 2, B). Time: B (0 s), C (0.1 s), D (0.2 s), E (0.3 s), F (22 s), G (22.1 s), H (22.2 s) and I (22.3 s). Arrowheads indicate different single red blood cells traveling along the capillary branch. Note blood flowing in vessels 1 and 2 (B–E), whereas, in (F)–(I), blood only flows in vessel 2. See Movie S1 for the full recording. An approximated time stamp for each snapshot is shown on the lower left corner of each image. Scale bars, 75 μm (A) and 20 μm (B–I).

(J) Quantification of blood flow velocity in vessels 1 and 2 (v1 and v2, B–I). Shown is islet blood flow velocity in monkey and mouse islets.

(K) Scatter data graph showing the blood flow speed in different capillaries in the monkey and mouse islet in vivo.

(L) Linear correlation between blood flow velocity and capillary diameter in mouse and monkey islets. Blood flow velocity was calculated by tracking the distance covered by single red blood cells (RBCs) over time and corrected by the imaging frame rate. For mice, n = 3 animals, n = 7 islets, and n = 146 RBCs. For monkeys,

(legend continued on next page)

compensated for by a reconfiguration of intra-islet blood perfusion via modulating the vasoconstriction and vasodilation of islet capillaries (Figures 3 and 4). This selective and fast adaptation of the islet blood supply would not require increasing the whole islet blood flow, thus protecting the islet from damaging hemodynamic stress.

Here we have monitored a critical aspect of primate islet function in vivo, underscoring the potential role of islet vasculature as an active and dynamic factor in islet physiology. This approach provides direct access to the complex interface between vasculature and islet endocrine cells.

EXPERIMENTAL PROCEDURES

Microscope Setup

All procedures were approved by the Institutional Animal Care and Use Committee (IACUC) of Singapore General Hospital and the Lee Kong Chian School of Medicine, Singapore. Monkeys (*Macaca fascicularis*), male, around 9–14 years old, were used in this study. The microscope used in this study is largely based on the Leica true confocal scanner (TCS) SP8 DM6000 confocal fixed stage (CFS) upright confocal and two-photon, laser-scanning, fixed-stage microscope and is fitted with a white-light laser, a Coherent Chameleon 2 Ti:Sapphire laser, and a Coherent optical parametric oscillator (OPO). The system has 5 detectors: 3 internal hybrid (HyD) and 2 photomultiplier (PMT) detectors and 2 external non-descanned HyD detectors. To accommodate the size of a monkey lying down, the microscope is fitted with a large imaging platform set on top of a high-precision scanning stage. This platform is supported by a mechanical jack that elevates the imaging platform and allows for coarse adjustments of the platform height, facilitating the positioning of the eye under the stereomicroscope (next to the microscope) or the microscope objective mount. The entire stage structure sits on top of rails that are used to slide the imaging platform and position the animal under the stereo- or two-photon microscope objective. When in position, the entire imaging platform is locked in place, and only the scanning stage mechanism can move freely in XY vectors. To accommodate the long traveling range of the imaging platform and the monkey's dimensions, the transmission illumination part was omitted from the microscope body to leave space for the monkey's head. The microscope body sits on top of an elevated anti-vibration platform supported by 4 pillars, which grants ample room to accommodate the imaging platform with a monkey inside the light protection box. The system is also equipped with an 8,000-Hz resonance scanner and a piezo Z drive for fast volumetric acquisitions. The light protection box contains openings on its side to allow the insertion/passage of lines for i.v. infusions and anesthesia or adjustment of the animal's position when in the box.

Ca^{2+} Biosensor Construction

pENTR1A.RIP2.GCaMP6s and pENTR1A.RIP2.GCaMP6f were generated by replacing the cDNA for EGFP in pENTR1A.RIP2.EGFP with that of GECI calmodulin GFP 6 slow proteins (GCaMP6s) obtained from pGP-CMV-GCaMP6s (Addgene, 40753). Internal ribosome entry site (IRES)-tdTomato was generated by introducing the cDNA of tdTomato downstream of the IRES sequence in pIRES (Clontech, Palo Alto, CA, USA). The IRES-tdTomato cassette was then introduced into pENTR1A.RIP2.GCaMP6s, thus creating pENTR1A.RIP2.GCaMP6s-IRES-tdTomato. All constructions were verified by DNA sequencing. The expression cassettes were transferred into the promoter-less adenovirus plasmid pAd/PL-DEST (Invitrogen, Carlsbad, CA, USA) by the Gateway technique. The ViraPower adenoviral expression system (Invitrogen) was used to generate replication-deficient adenoviruses, which were used for transduction of islet cells.

In Vitro Imaging of Islet Ca^{2+} Dynamics

To confirm that the isolated islets are functional prior to ACE transplantation, we carried out in vitro imaging of cytoplasmic free Ca^{2+} concentration ($[Ca^{2+}]_i$) changes in response to a glucose challenge. A fluorescent wide-field microscope (Leica DMI6000B) was used for $[Ca^{2+}]_i$ imaging of islets 2–6 days after infection with an adenovirus containing the genetically encoded Ca^{2+} sensor GCaMP6s under the control of the rat insulin-2 gene promoter (described above). For imaging, single islets were attached to a glass coverslip using a peptide hydrogel (Corning Life Sciences, 354250) in a low-volume open recording chamber (Warner Instruments), with the whole system maintained at 37°C. Islets were incubated for 2 hr prior to imaging in buffer containing 125 mM NaCl, 5.9 mM KCl, 2.56 mM $CaCl_2$, 1 mM $MgCl_2$, 25 mM 4-(2-hydroxyethyl)-1-piperazineethanesulfonic acid (HEPES), and 3 mM glucose (pH 7.4). Glucose concentrations of 11 mM or 16.7 mM were used for islet stimulation, followed by buffer containing an additional 25 mM KCl to give a maximum depolarizing response. GCaMP6s fluorescence was measured using excitation from a xenon lamp (Sutter DG-4) and GFP filter set (excitation, 450–490 nm; dichroic, 495 nm; emission, 500–550 nm). Responses were quantified for each cell as the measured change in fluorescence divided by baseline fluorescence ($\Delta F/F0$).

Partial Pancreatectomy

Animals were sedated with an intra-muscular (IM) injection of ketamine (10 mg/kg) and isoflurane at 3%–5%. After induction, the animal was intubated with the appropriate endotracheal tube using a laryngoscope and maintained anesthetized with 1%–2% isoflurane. Depth of anesthesia was monitored by breathing frequency and absence of reflexes (e.g., palpebral reflex, toe pinch). Animals received a preoperative analgesic (carporfen, 4 mg/kg, subcutaneously [s.c.]) and antibiotic (enrofloxacin, 5 mg/kg, IM) treatment. The abdomen was shaved and surgically prepped with alcohol, chlorhexidine, and povidone iodine. Under general anesthesia, a ventral midline laparotomy was performed, and the pancreas was identified and exposed. If needed, the surgeon removed excess adipose tissue covering the pancreas. Next, the splenic artery that supplies the tail of the pancreas was ligated, and less than 50% (usually 20%–30%) of the pancreas was carefully removed. After completion of the partial pancreatectomy procedure, the abdomen was closed with an absorbable suture (Monosyn 2-0), and the animal was monitored and allowed to recover from anesthesia. Adequate coagulation and minimum hemorrhage were ensured by using a combination of diathermy and adequate ligation of the splenic artery and its branches. There were no restrains on the animals during the recovery period. Monkeys were monitored for pain, bleeding of the surgical site, urination, and appetite during the next 3–7 days by trained veterinarians. All animals received post-operative analgesics and antibiotics (described above) for the next 3–7 days.

Islet Isolation

Islet isolation was performed as described previously with modifications (Berman et al., 2009). Briefly, the resected tail piece of the pancreas (20%–30% of

n = 2 animals, n = 3 islets, and n = 162 RBCs. Data from mice were acquired on a single day, and data from monkeys were acquired over 3 independent imaging sessions for two animals. Data are from fasted animals; monkeys were fasted for more than 8 hr and mice between 4–6 hr. Shown is sphincter-like regulation of islet blood flow.

(M–P) Snapshots of time-lapse confocal microscopy showing the progression of focalized capillary occlusion in monkey islets in vivo. Time: M (0 s), N (2.4 s), O (6.5 s), and P (24 s).

(Q) Quantification of the diameter of capillaries shown in (M)–(P) at three different regions of interest (ROIs) (a–f) per capillary. Scale bars, 25 μm.

(R) Illustration representing the possible mechanism and consequences of blood flow regulation in the primate islet. The open capillary has continuous blood flow, and endocrine cells lining this capillary branch have access to fresh blood supply. When triggered, the mural cell contracts and constricts select capillaries, and blood flow is redirected to suit different cellular needs, such as cells with a higher metabolic rate.

In (K) and (L), data are presented as mean ± SD.

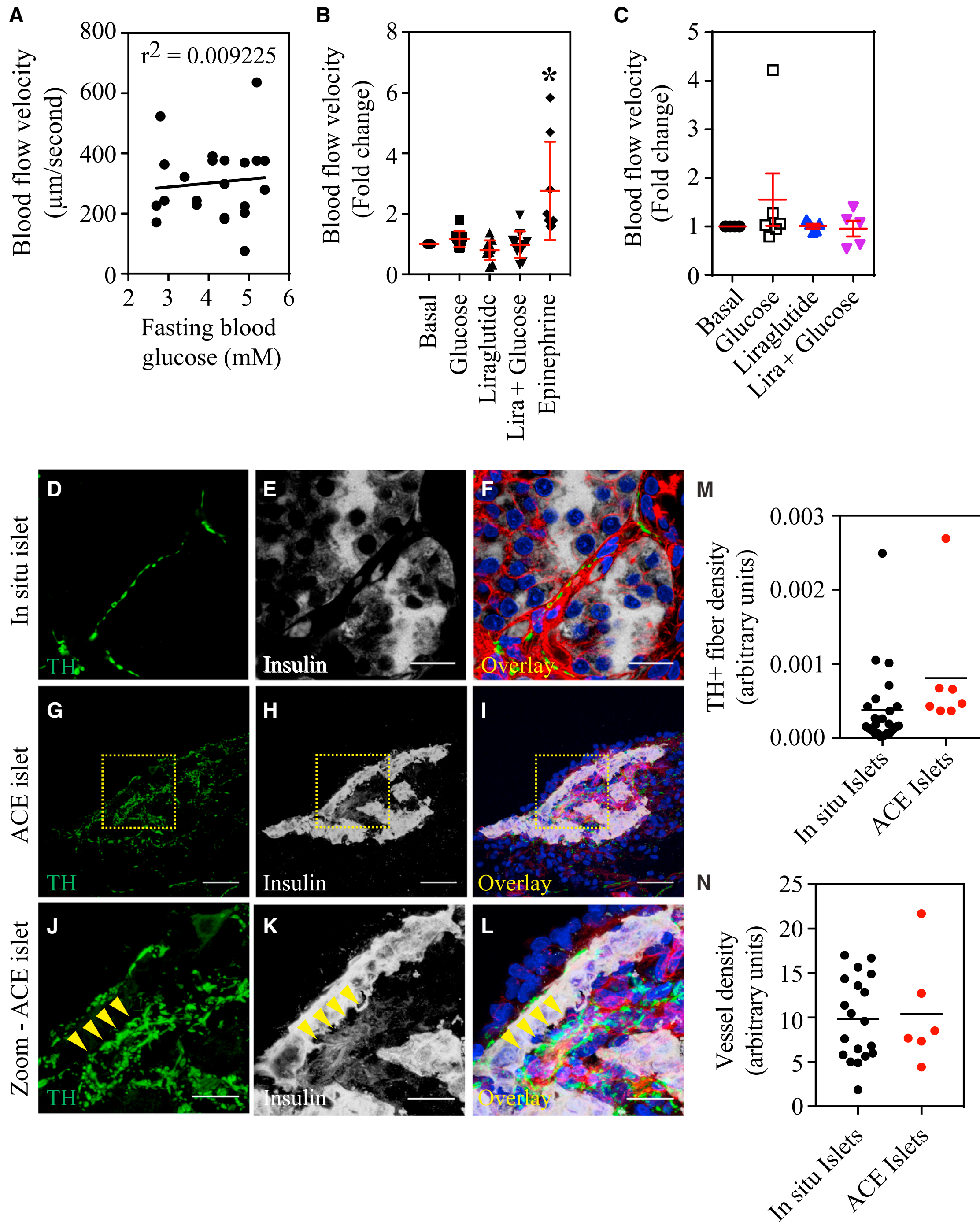

Figure 4. Primate Islet Blood Flow Is Not Sensitive to Glucose or Liraglutide

(A) Basal blood flow velocity does not depend on fasting blood glucose level. Each data point on the graph indicates the average speed of RBCs (n = 5–16 cells), quantified in different capillaries (n = 8–11) in n = 2 animals.

(B) Blood flow velocity was measured in islet capillaries as described above, before and after injecting i.v. liraglutide (1 mg/kg of BW), saline, glucose (0.5 g/kg of BW), or epinephrine (0.15 mg, one single shot).

(C) Blood flow velocity was measured in iris capillaries as described above, before and after injecting liraglutide (1 mg/kg of BW) or saline and glucose (0.5 g/kg of BW).

(D–L) Sympathetic nerve fibers contact mainly the blood vessels in islets in situ (D–F) and engrafted on the iris (G–L). In (J), yellow arrowheads indicate TH+ nerve fibers innervating the islet vasculature.

(legend continued on next page)

the total pancreas) was cannulated through the opened duct at the incision site using a 24G cannula. Next, 11–16 mL of 0.47 mg/mL liberase enzyme mix (Roche, 5401020001) diluted in Hank's balanced salt solution (HBSS) (Gibco, 24020-117) with 17 mM HEPES was injected carefully, and the tissue was distended. The liberase injection was repeated twice, reusing the excess of the same enzyme-containing buffer, and once more by random injections in the resected pancreas using a 19G needle. The distended tissue was trimmed into 5–6 small pieces using surgical scissors and placed inside a 50-mL Ricordi chamber for its enzymatic digestion. At different time points, we collected samples from the chamber, and when islets were clearly visualized as being separated from the surrounding acinar tissue, the digestion was stopped by addition of cold RPMI (Gibco, 11835-055) containing 10% heat-inactivated fetal bovine serum (FBS) (Gibco, 10270-106), 12.5 mM HEPES, and 10 mM nicotinamide (RonaCare, 130179). The digested pancreas was washed twice in cold RPMI by gentle centrifugation at 280 × *g* for 5 min at 4°C with brakes at medium level. The resulting pellet was re-suspended in Ficoll, 1.110 g/mL (obtained by adding 2 mL of 1.137 g/mL stock polysucrose solution [Cellgro, C05/99-662-CVS] to 75 mL of 1.108 g/mL [Cellgro, C05/99-692-CIS]). Next we prepared a discontinuous gradient by loading on top of the sample the following layers in order: Ficoll, 1.096 g/mL (Cellgro, C05/99-691-CIS); Ficoll, 1.037 g/mL (Cellgro, C05/99-690-CIS); and plain HBSS layers. The Ficoll gradient was centrifuged at 380 × *g* for 15 min at 4°C (without brakes). We collected the interface between 1.096 and 1.037 (which contains the pure islet fraction), diluted it in cold RPMI (10% FBS, 12.5 mM HEPES, and 10 mM nicotinamide), and washed it twice by centrifugation at 270 × *g* for 5 min at 4°C with brakes at medium level. Finally, islets were re-suspended in Connaught Medical Research Laboratories (CMRL) medium (Gibco, 11530037) containing 5% monkey serum (obtained from the same animal), 12.5 mM HEPES, 10 mM nicotinamide, 2 mM L-glutamine (Gibco, 25030-081), and 100 U/mL of penicillin/streptomycin mix (Gibco, 15140122) and incubated at 22°C until further use or immediately infected with adenoviral particles and kept at 37°C.

Islet Transplantation into the Anterior Chamber of the Monkey's Eye

Anesthesia was induced with an injection (IM) of ketamine (10–20 mg/kg). When the animal was under deep anesthesia, it was intubated with the appropriate endotracheal tube using a laryngoscope. An i.v. line was established by placing an appropriately sized catheter in the left or right cephalic vein. Warm saline solution (0.9% NaCl) was administered i.v. by slow drip throughout the duration of the procedure. Next, the animal was transported to the transplantation and in vivo imaging room, and, upon arrival, the animal was aseptically prepared for surgery. The animal was restrained on a surgical table in the room using sterile ropes. After confirming that the animal was under deep anesthesia, it was gavaged with 1 capsule of Diamox sequels (acetazolamide, 500 mg). Then the intraocular pressure (IOP) of the eye receiving the transplant was measured using a tonometer. One drop of 1% xylocaine was put onto the eye as a topical anesthetic to reduce possible discomfort to the animals during the IOP measurement procedure. Eight measurements were made to obtain a valid mean value. Next, we applied pilocarpine (1%, one drop in each eye) prior to the transplantation of islets to constrict the pupil and maximize the exposed area of the iris. We applied topical anesthesia (1% xylocaine) to the ocular surface before surgery, and the cul-de-sac and eyelids were aseptically cleaned with Betadine (10% solution). The right or left eye was draped for surgery, and a lid speculum was placed to retract the eyelids. A paracentesis/corneal self-sealing incision was performed at the superior temporal and nasal quadrants alternatively with a 23G needle. Great care was taken not to damage the iris and to avoid bleeding. The islets were suspended in 200 μL of PBS and transplanted using a 25G blunt cannula, making sure the islets were distributed throughout the surface area of the iris to favor their engraftment. To avoid reflux of islets from the anterior chamber, the intraocular pressure was allowed to subside by waiting 10–20 s with the cannula in place and then resuming the injection. Islets were repositioned on top of the iris and out of the pupil using the blunt cannula to prevent disturbing the eyesight. Immediately after the injection, a drop of ophthalmologic gel (Viscotears, 2 mg/mL) was put on the eye to prevent desiccation. The animal was kept anesthetized in a resting horizontal position for 2–2.5 hr to allow the islets to settle down by gravity on the surface of the iris and favor engraftment. Then, one drop of Tobrex (0.3% tobramycin) and one drop of Predforte (1% prednisolone acetate) were administered. Subsequent to surgery, the animal was given enrofloxacin prior to recovery (5 mg/kg, IM), and buprenorphine (0.01 mg/kg, IM) after recovering from anesthesia. Finally, the animal was transported back to its cage after full recovery.

Complete Examination of the Transplanted and Non-transplanted Eyes Using the Slit Lamp Exam

Monkeys were anesthetized by IM injection of ketamine (20 mg/kg body weight) and acepromazine maleate (0.25 mg/kg body weight). The airway, respiration, and pulse were monitored during all procedures. One to two drops of 1% xylocaine was used as a topical anesthetic to reduce possible discomfort to the animals during the procedure. Pupils were dilated with 2.5% phenylephrine hydrochloride and 1% tropicamide drops (Alcon Laboratories, Frenchs Forest, NSW, Australia) for retinal imaging. Five monkeys were used for this study, two non-transplanted and three transplanted. For IOP measurements, the monkeys were lightly anesthetized with ketamine at 5 mg/kg body weight. The topical anesthesia was applied as mentioned above. IOP was measured via tonometer (Tono-Pen XL, Reichert Technologies, Depew, NY) at 2–4 p.m. The procedure took about 5 min for each monkey. After the transplant, IOP in both eyes of all animals was measured once daily for 3 consecutive days. Six to eight IOP measurements were made to ensure that an average IOP measurement was attained each time. For clinical examination, we performed a visual daily inspection of all eyes after injections or topical administration for signs of conjunctival irritation, inflammation, or infection at the injection site. Slit lamp microscopic examination of the exterior, anterior chamber, and posterior chamber of the eyes was performed before the injections and after transplantation. The monkeys were also monitored for any gross changes such as eye discharge, squinting, or abnormal behavior suggesting pain or severe discomfort. Anterior chamber and vitreous cell scores were determined for the examined eyes using a slit lamp biomicroscope. The score assigned was as follows: no cells observed, 0; 1–5 cells per single field of focused beam, 0.5+; 5–25 cells, 1+; 25–50 cells, 2+; 50–100 cells, 3+; more than 100 cells, 4+. For color fundus photography (CFP) and fluorescein fundus angiography (FFA), the monkey's fundi of both transplanted, contra-lateral control, and naive control eyes were imaged with a fundus camera (Topcon, Tokyo, Japan) using a digital camera on days 126 (monkey C-282) or 231 (monkeys B-116 and B-159) after transplantation. FFA was done upon completion of CFP and using the same cameras but with excitation and barrier filters added. FFA was performed by i.v. injection of 10% sodium fluorescein (0.1 mL/kg body weight), with images taken between 10 s and 10 min after dye injection to assess the retinal and choroidal microvasculature. For posterior segment optical coherence tomography (OCT), we used low-coherence interferometry to produce a two-dimensional image of optical scattering from internal tissue microstructures in a way that is analogous to ultrasonic pulse-echo imaging. The microstructure of the retinal layers was examined using a Heidelberg Spectralis retinal tomography Spectral Domain-Optical Coherence Tomography (HRT SD-OCT) (Heidelberg, Germany). The system provides an in vivo histological section of the retina and choroid, which was used to detect any changes in the microstructure of the retina, including the retinal pigment epithelium (RPE) and macular and choroidal thickness. For statistical analysis, significance was set at 0.05 levels. Student's t test was used to compare transplanted and control eyes.

(M) Quantification of relative TH-positive sympathetic nerve fiber density in in situ (n = 24 islets total, n = 5 monkeys) (black circles) and ACE islets (n = 7 islets total, n = 2 monkeys) (red circles).
(N) Vessel density quantification in islets in situ (n = 24 islets, n = 5 monkeys) (black circles) and engrafted in the eye (n = 6 islets, n = 2 monkeys) (red circles). Images show 20-μm sections immunostained with antibodies against insulin (gray), phalloidin (red), and TH (green). DAPI staining is shown in blue. Scale bars, 10 μm (D–F and J–L) and 25 μm (G–I). In (B) and (C), data are presented as mean ± SD.

In Vivo Two-Photon Imaging of the Engrafted Islets' Vascularization

First, the animal was anesthetized with an IM injection of ketamine (10 mg/kg) and intubated as described above. To lower the animal's heart rate and minimize movement during imaging, the animal was given medetomidine (0.1 mg/kg, i.v.). Next, the animal was placed carefully on top of the scanning stage and a heated mat, used to maintain the body temperature, and restrained with a custom-built head holder. The animal was maintained under anesthesia with 1%–3% isoflurane throughout the imaging procedure. The eyelids were retracted with a lid speculum, and the eye was immobilized with a custom-build eye holder (Figures 2C and 2D). Two drops of PBS were placed on top of the eye that was not being imaged to prevent corneal dehydration during the imaging procedure. The eye containing the islets was immersed in imaging gel (Viscotears, 2 mg/mL), and the animal was placed under the microscope objective. Next, the mounted objective (20×/0.5 numerical aperture [NA] or 25×/0.95 NA) was lowered carefully using fine z-drive controls until the iris and the focal plane were in sight. To visualize the islet (and iris) vessels, the animal was injected with 150 kDa FITC-labeled dextran (50 mg/kg, Sigma, St. Louis, MO). Islets were identified by their spherical shape and/or intricate vascularization pattern. To facilitate the repeated observation of a particular islet, we mapped the islet's position on the iris based on images acquired with a stereomicroscope after engraftment (Figures 1E–1H). After identifying the islet of interest, we performed two-photon microscopy of the islet ultra-structure and vascularization using a Chameleon II two-photon Ti:Sapphire laser and external non-descanned detectors (NDDs). To image the vessels, we excited FITC-labeled dextran molecules with a 920-nm wavelength and collected FITC emission with an non-descanned detector fitted with a 500- to 550-nm emission filter. It was not possible to image the engrafted islet mass using light scatter with a 633-nm excitation laser line (Ilegems et al., 2015) because of the intrinsic optical properties of the monkey iris. Instead, we imaged the islet ultrastructure indirectly with the 920-nm wavelength, which results in excited fluorescent emission from a thin pigmented layer that sits on top of the islet graft (Figure S3I) and that can be detected with an non-descanned detector fitted with a 560- to 605-nm filter. As a result, vessels and islet ultrastructure were imaged simultaneously with a single excitation line. All imaging sessions were performed with the use of a piezo z-drive and an 8,000-Hz resonance scanner. Laser intensity was minimized to avoid damage to the islet, iris, retina, or cornea. Images describing the islet vascularization pattern were acquired in XYZ with a 512 × 512 pixel format, whereas recordings of blood flow dynamics were acquired in XYT with an approximate 400 × 400 pixel format to maximize scanning speeds and temporal resolution. When the imaging session was over, the animal was carefully removed from the microscope, and its eyes were washed with PBS. Finally, the lid speculum and the ventilated anesthesia were removed, and the animal was allowed to recover in a dedicated recovery room. After full recovery, the animal was transported back to its housing cage.

Longitudinal Measurement of Blood Flow Velocity

Capillaries were labeled with 50 mg/kg of FITC-labeled 150-kDa dextran molecules. Red blood cells were visualized as moving shadows in the labeled capillaries. We took time-lapse images from different vascular branches in engrafted islets or the iris with a temporal resolution of 17–32 frames/s. Before the start of the experiment, we mapped the position of 2–3 different islet or iris capillaries and measured the basal velocity of circulating red blood cells. Next, we injected liraglutide (Victoza, Novo Nordisk) at a dose (1 mg/kg of body weight [BW]) within the range recommended for humans and higher than the dose used in a humanized mouse model (0.3 mg/kg/day) (Abdulreda et al., 2016) or saline (0.9% NaCl) i.v., and, 2 min later, we measured the red blood cell velocity in the same capillaries as mapped before. Next, glucose (0.5 M/kg of BW) was injected, and, after 2 min, we measured the red blood cell velocity as described above. As a positive control, we measured islet blood flow before and immediately after injecting epinephrine (0.15 mg, single dose) i.v. For each capillary and treatment condition (e.g., liraglutide), we calculated the average velocity of 5–16 different circulating red blood cells using ImageJ and the plugin MTrackJ (Meijering et al., 2012). For the data analysis, the raw red blood cell velocity in microns per second for each capillary and treatment condition was normalized to initial basal velocity and plotted as fold change. Statistical significance was evaluated with Student's t test.

Immunohistochemistry, Image Alignment, and Analysis after Acquisition

Immunohistochemistry and confocal imaging of stained slides were performed as by Rodriguez-Diaz et al. (2011b). For histological analysis of the islets engrafted in the monkey eye, after euthanasia, the eye containing the transplanted islets was removed, fixated in 4% paraformaldehyde (PFA) for 48 hr, and preserved in 30% sucrose at 4°C. Next, the iris was carefully separated from the rest of the eye globe, cryo-preserved, and sectioned. All images were processed and quantified in ImageJ software. Blood flow speed was quantified by tracking single red blood cells with the ImageJ plugin MtrackJ (Meijering et al., 2012). Quantification of TH fiber density in in situ (n = 24 islets, n = 5 monkeys) and ACE islets (n = 7, n = 2 monkeys) was done using Fiji/ImageJ. First, the TH intensity signal for each maximum projection image was thresholded to remove background and autofluorescence. This step made sure that only sympathetic fibers were quantified. Next, we calculated the relative pixel density (in percent) of TH-positive pixels in the islet and normalized this information by the islet area (in square micrometers). Quantification of the vascular density of the engrafted islets was done by measuring the pixel intensity of the FITC channel within the islet region, determined from image stacks acquired with confocal and two-photon microscopy. Next, the data were normalized to account for different excitation/detection efficiencies between the imaging protocols used. Quantification of the vascular density in ACE and in situ islet sections was done using ImageJ. In brief, the islet area (as determined by insulin staining) and the area occupied by clearly identified f-actin-rich capillaries was calculated. Next, the fraction of the islet area occupied by the islet vasculature was calculated and plotted using GraphPad Prism. The in vivo vascular diameter was measured in at least 3 different single stacks of z stack acquisitions from engrafted islets from 2 different animals. Image drifts from heartbeat, breathing, and gradual movement of the iris were corrected by using a custom-written 3D image registration plugin that runs on ImageJ and is based on a subpixel image registration algorithm (Thévenaz et al, 1998). Here, multicolor z stack images were recursively aligned according to the template slice, and a projection was performed (Figure S2).

Statistical Analysis

All statistical analyses were done using GraphPad Prism software. In multi-condition experiments (i.e., Figures 2G and 4), the data from each capillary were normalized to their respective basal levels. Next, the data were analyzed using one-way ANOVA with Dunnett's multi-comparison test to compare all experimental conditions with the basal conditions. For experiments that had data from only 2 animals per condition (i.e., Figures 4M and 4N), no statistical analysis was performed, and so the data plotted are shown without error bars, and all points are shown. For all tests, $p < 0.05$ was considered significant, and no data points were excluded from the analysis.

SUPPLEMENTAL INFORMATION

Supplemental Information includes three figures, one table, and four movies and can be found with this article online at http://dx.doi.org/10.1016/j.celrep.2017.07.039.

AUTHOR CONTRIBUTIONS

J.A.D. and R.A.D. contributed to the conception and design of the study as well as acquisition, analyses, and interpretation of data and writing of the manuscript. X.Z., O.V.S., M.C., R.R.D., M.F., M.K., I.L., S.B.B.T., Y.A., G.J.A., and V.A.B. contributed to the acquisition of data and critical revision of the manuscript. P.O.B. was the originator of the idea underlying this study and contributed to its conception and design as well as writing of the manuscript. All authors approved the final version. P.O.B. is the guarantor of this work.

ACKNOWLEDGMENTS

We thank Bryan Ogden and the veterinary team at SEMC, SingHealth, for technical support with animal care and handling. This work was supported by a Lee

Kong Chian School of Medicine, Nanyang Technological University start-up grant (to P.O.B.) M4230003, the Swedish Research Council, the Family Erling-Persson Foundation, the Novo Nordisk Foundation, the Stichting af Jochnick Foundation, the Swedish Diabetes Association, the Scandia Insurance Company, the Diabetes Research and Wellness Foundation, Berth von Kantzow's Foundation, the Strategic Research Program in Diabetes at Karolinska Institutet, the ERC ERC-2013-AdG 338936-BetaImage, and the Knut and Alice Wallenberg Foundation. R.A.D. was supported by the Nanyang Structural Biology Institute (NISB) L0408020 and by an AXA Research Fund postdoctoral fellowship, L0484201. V.A.B. is supported by National Medical Research Council, Singapore grant NMRC/CG/015/2013. P.O.B. is co-founder and CEO of Biocrine, an unlisted biotech company that is using the ACE technique as a research tool.

Received: January 5, 2017
Revised: May 5, 2017
Accepted: July 14, 2017
Published: August 8, 2017

REFERENCES

Abdulreda, M.H., Rodriguez-Diaz, R., Caicedo, A., and Berggren, P.-O. (2016). Liraglutide Compromises Pancreatic β Cell Function in a Humanized Mouse Model. Cell Metab. *23*, 541–546.

Almaça, J., Molina, J., Arrojo E Drigo, R., Abdulreda, M.H., Jeon, W.B., Berggren, P.-O., Caicedo, A., and Nam, H.G. (2014). Young capillary vessels rejuvenate aged pancreatic islets. Proc. Natl. Acad. Sci. USA *111*, 17612–17617.

Arrojo e Drigo, R., Ali, Y., Diez, J., Srinivasan, D.K., Berggren, P.O., and Boehm, B.O. (2015). New insights into the architecture of the islet of Langerhans: a focused cross-species assessment. Diabetologia *58*, 2218–2228.

Bader, E., Migliorini, A., Gegg, M., Moruzzi, N., Gerdes, J., Roscioni, S.S., Bakhti, M., Brandl, E., Irmler, M., Beckers, J., et al. (2016). Identification of proliferative and mature β-cells in the islets of Langerhans. Nature *535*, 430–434.

Berman, D.M., O'Neil, J.J., Coffey, L.C.K., Chaffanjon, P.C.J., Kenyon, N.M., Ruiz, P., Jr., Pileggi, A., Ricordi, C., and Kenyon, N.S. (2009). Long-term survival of nonhuman primate islets implanted in an omental pouch on a biodegradable scaffold. Am. J. Transplant. *9*, 91–104.

Brissova, M., Fowler, M.J., Nicholson, W.E., Chu, A., Hirshberg, B., Harlan, D.M., and Powers, A.C. (2005). Assessment of human pancreatic islet architecture and composition by laser scanning confocal microscopy. J. Histochem. Cytochem. *53*, 1087–1097.

Brown, R.J., and Rother, K.I. (2008). Effects of beta-cell rest on beta-cell function: a review of clinical and preclinical data. Pediatr. Diabetes *9*, 14–22.

Cabrera, O., Berman, D.M., Kenyon, N.S., Ricordi, C., Berggren, P.-O., and Caicedo, A. (2006). The unique cytoarchitecture of human pancreatic islets has implications for islet cell function. Proc. Natl. Acad. Sci. USA *103*, 2334–2339.

Donáth, T., and Adeghate, E. (1988). Re-innervation of pancreatic tissue implants in normal and in sympathetically denervated eyes of rats. Acta Morphol. Hung. *36*, 147–154.

Ehringer, H., and Konzett, H. (1962). Analysis of the vasodilator effect of adrenaline on the skeletal muscle vessels of man. Nature *194*, 1184.

Hall, C.N., Reynell, C., Gesslein, B., Hamilton, N.B., Mishra, A., Sutherland, B.A., O'Farrell, F.M., Buchan, A.M., Lauritzen, M., and Attwell, D. (2014). Capillary pericytes regulate cerebral blood flow in health and disease. Nature *508*, 55–60.

Ilegems, E., Dicker, A., Speier, S., Sharma, A., Bahow, A., Edlund, P.K., Leibiger, I.B., and Berggren, P.-O. (2013). Reporter islets in the eye reveal the plasticity of the endocrine pancreas. Proc. Natl. Acad. Sci. USA *110*, 20581–20586.

Ilegems, E., van Krieken, P.P., Edlund, P.K., Dicker, A., Alanentalo, T., Eriksson, M., Mandic, S., Ahlgren, U., and Berggren, P.O. (2015). Light scattering as an intrinsic indicator for pancreatic islet cell mass and secretion. Sci. Rep. *5*, 10740.

Jacques-Silva, M.C., Correa-Medina, M., Cabrera, O., Rodriguez-Diaz, R., Makeeva, N., Fachado, A., Diez, J., Berman, D.M., Kenyon, N.S., Ricordi, C., et al. (2010). ATP-gated P2X3 receptors constitute a positive autocrine signal for insulin release in the human pancreatic β cell. Proc. Natl. Acad. Sci. USA *107*, 6465–6470.

Jansson, L., and Hellerström, C. (1983). Stimulation by glucose of the blood flow to the pancreatic islets of the rat. Diabetologia *25*, 45–50.

Lammert, E. (2001). Induction of Pancreatic Differentiation by Signals from Blood Vessels. Science *294*, 564–567.

Meijering, E., Dzyubachyk, O., and Smal, I. (2012). Methods for cell and particle tracking. Methods Enzymol. *504*, 183–200.

Nyman, L.R., Wells, K.S., Head, W.S., McCaughey, M., Ford, E., Brissova, M., Piston, D.W., and Powers, A.C. (2008). Real-time, multidimensional in vivo imaging used to investigate blood flow in mouse pancreatic islets. J. Clin. Invest. *118*, 3790–3797.

Nyman, L.R., Ford, E., Powers, A.C., and Piston, D.W. (2010). Glucose-dependent blood flow dynamics in murine pancreatic islets in vivo. Am. J. Physiol. Endocrinol. Metab. *298*, E807–E814.

Nyqvist, D., Speier, S., Rodriguez-Diaz, R., Molano, R.D., Lipovsek, S., Rupnik, M., Dicker, A., Ilegems, E., Zahr-Akrawi, E., Molina, J., et al. (2011). Donor islet endothelial cells in pancreatic islet revascularization. Diabetes *60*, 2571–2577.

Perez, V.L., Caicedo, A., Berman, D.M., Arrieta, E., Abdulreda, M.H., Rodriguez-Diaz, R., Pileggi, A., Hernandez, E., Dubovy, S.R., Parel, J.M., et al. (2011). The anterior chamber of the eye as a clinical transplantation site for the treatment of diabetes: a study in a baboon model of diabetes. Diabetologia *54*, 1121–1126.

Petzold, G.C., and Murthy, V.N. (2011). Role of astrocytes in neurovascular coupling. Neuron *71*, 782–797.

Pound, L.D., Kievit, P., and Grove, K.L. (2014). The nonhuman primate as a model for type 2 diabetes. Curr. Opin. Endocrinol. Diabetes Obes. *21*, 89–94.

Provenza, D.V., and Scherlis, S. (1959). Demonstration of muscle sphincters as a capillary component in the human heart. Circulation *20*, 35–41.

Rodriguez-Diaz, R., Dando, R., Jacques-Silva, M.C., Fachado, A., Molina, J., Abdulreda, M.H., Ricordi, C., Roper, S.D., Berggren, P.-O., and Caicedo, A. (2011a). Alpha cells secrete acetylcholine as a non-neuronal paracrine signal priming beta cell function in humans. Nat. Med. *17*, 888–892.

Rodriguez-Diaz, R., Abdulreda, M.H., Formoso, A.L., Gans, I., Ricordi, C., Berggren, P.O., and Caicedo, A. (2011b). Innervation patterns of autonomic axons in the human endocrine pancreas. Cell Metab. *14*, 45–54.

Rodriguez-Diaz, R., Speier, S., Molano, R.D., Formoso, A., Gans, I., Abdulreda, M.H., Cabrera, O., Molina, J., Fachado, A., Ricordi, C., et al. (2012). Noninvasive in vivo model demonstrating the effects of autonomic innervation on pancreatic islet function. Proc. Natl. Acad. Sci. USA *109*, 21456–21461.

Speier, S., Nyqvist, D., Cabrera, O., Yu, J., Molano, R.D., Pileggi, A., Moede, T., Köhler, M., Wilbertz, J., Leibiger, B., et al. (2008). Noninvasive in vivo imaging of pancreatic islet cell biology. Nat. Med. *14*, 574–578.

Svensson, A.M., Östenson, C.-G., Efendic, S., and Jansson, L. (2007). Effects of glucagon-like peptide-1-(7-36)-amide on pancreatic islet and intestinal blood perfusion in Wistar rats and diabetic GK rats. Clin. Sci. *112*, 345–351.

Thévenaz, P., Ruttimann, U.E., and Unser, M. (1998). A pyramid approach to subpixel registration based on intensity. IEEE Trans Image Process *7*, 27–41.

Tucker, D.C., and Torres, A. (1992). Adrenal hormones interact with sympathetic innervation to modulate growth of embryonic heart in oculo. Am. J. Physiol. *262*, H318–H325.

Unger, R.H., and Orci, L. (2010). Paracrinology of islets and the paracrinopathy of diabetes. Proc. Natl. Acad. Sci. USA *107*, 16009–16012.

Visa, M., Alcarraz-Vizán, G., Montane, J., Cadavez, L., Castaño, C., Villanueva-Peñacarrillo, M.L., Servitja, J.M., and Novials, A. (2015). Islet amyloid polypeptide exerts a novel autocrine action in β-cell signaling and proliferation. FASEB J. *29*, 2970–2979.

Watts, M., Ha, J., Kimchi, O., and Sherman, A. (2016). Paracrine Regulation of Glucagon Secretion: The β-α-δ Model. Am. J. Physiol. Endocrinol. Metab. *310*, E597–E611.

Wu, L., Olverling, A., Huang, Z., Jansson, L., Chao, H., Gao, X., and Sjöholm, Å. (2012). GLP-1, exendin-4 and C-peptide regulate pancreatic islet microcirculation, insulin secretion and glucose tolerance in rats. Clin. Sci. *122*, 375–384.

Yan-Do, R., Duong, E., Manning Fox, J.E., Dai, X., Suzuki, K., Khan, S., Bautista, A., Ferdaoussi, M., Lyon, J., Wu, X., et al. (2016). A glycine-insulin autocrine feedback loop enhances insulin secretion from human β-cells and is impaired in type 2 diabetes. Diabetes *65*, 2311–2321.